

A model for the linear stability of the interface between aqueous humor and vitreous substitutes after vitreoretinal surgery

Krystyna Isakova, Jan O. Pralits, Rodolfo Repetto, and Mario R. Romano

Citation: *Physics of Fluids* (1994-present) **26**, 124101 (2014); doi: 10.1063/1.4902163

View online: <http://dx.doi.org/10.1063/1.4902163>

View Table of Contents: <http://scitation.aip.org/content/aip/journal/pof2/26/12?ver=pdfcov>

Published by the [AIP Publishing](#)

Articles you may be interested in

[Rapid 3D human ribcage and kidney modeling for transcatheter HIFU surgery](#)

AIP Conf. Proc. **1503**, 95 (2012); 10.1063/1.4769924

[A model for the human tear film with heating from within the eye](#)

Phys. Fluids **24**, 062103 (2012); 10.1063/1.4723870

[Modeling the interactions between compliant microcapsules and pillars in microchannels](#)

J. Chem. Phys. **127**, 034703 (2007); 10.1063/1.2753150

[Mechatronics Interface for Computer Assisted Prostate Surgery Training](#)

AIP Conf. Proc. **854**, 160 (2006); 10.1063/1.2356434

[History of shock wave lithotripsy](#)

AIP Conf. Proc. **524**, 23 (2000); 10.1063/1.1309176



A model for the linear stability of the interface between aqueous humor and vitreous substitutes after vitreoretinal surgery

Krystyna Isakova,¹ Jan O. Pralits,^{1,a)} Rodolfo Repetto,¹
 and Mario R. Romano²

¹*Department of Civil, Chemical and Environmental Engineering, University of Genoa, Genoa, Italy*

²*Istituto Clinico Humanitas, Milano, Italy*

(Received 15 June 2014; accepted 10 November 2014; published online 25 November 2014)

We consider the motion of two immiscible viscous fluids induced by periodic oscillations of a flat solid surface along its plane. The interface between the two fluids is parallel to the solid wall; one fluid occupies the region between the wall and the interface and the other extends from the interface to infinity. We study numerically the linear stability of the interface with respect to two-dimensional perturbations using the normal mode analysis and assuming quasi-steady flow conditions. The analysis is motivated by the need of understanding the behavior of vitreous substitutes inserted in the vitreous chamber of the eye after vitrectomy. This is a common surgical procedure adopted to treat retinal detachments, whereby the vitreous humor is removed from the eye and replaced by fluids immiscible with water. Owing to their hydrophobic nature, vitreous substitutes coexist in the vitreous chamber with a certain amount of aqueous humor (the fluid produced in the anterior part of the eye) and, typically, a thin layer of aqueous separates the tamponade fluid from the retina. A common problem with this treatment is that, in some cases, the interface between the two fluids breaks down and this might eventually lead to the generation of an emulsion. It is believed that mechanics plays an important role in this process but the problem remains very poorly understood. We find that instability of the interface is possible in a range of parameters that is relevant for the problem that motivated the present analysis. This suggests that shear instability is likely a possible mechanism triggering the onset of vitreous substitutes–aqueous interface instability. © 2014 AIP Publishing LLC. [<http://dx.doi.org/10.1063/1.4902163>]

I. INTRODUCTION

Retinal detachment (RD) occurs when the sensory layer of the retina detaches from the retinal pigment epithelium.¹ This is a serious condition that might lead to permanent loss of vision and needs immediate treatment. A commonly adopted surgical procedure to treat RD is vitrectomy: the vitreous body is removed from the vitreous chamber and replaced with a “vitreous substitute.” Various fluids can be used after vitrectomy, depending on the particular condition of the patient. In this paper, we focus on vitreous substitutes that are immiscible with water. In this category fall silicon oils, perfluorocarbon liquids, and semifluorinated alkane liquids. Mechanical properties, indications for adoption, and main complications associated with the existing vitreous substitutes are extensively described in the literature.^{2–4}

The primary role of vitreous substitutes is to interrupt the communication that was established through the retina break between the subretinal space/retinal pigment epithelial cells and the pre-retinal space. Depending on the location of the retinal damage, tamponade fluids with densities

^{a)} Author to whom correspondence should be addressed. Electronic mail: jan.pralits@unige.it

either smaller (for breaks in the superior part of the chamber) or larger than the aqueous density can be adopted.

At present no vitreous substitute exists that can be left indefinitely in the vitreous chamber, since various complications might arise. In particular, the interface between the vitreous substitute and the aqueous humor might break down and, eventually, an emulsion of droplets might form in the aqueous. This can lead to various postoperative complications, including cataract, keratopathy, and glaucoma.⁵

Owing to the hydrophobic properties of vitreous substitutes, the fluid might not be in direct contact with the retina and some aqueous humor is likely to line the wall of the eye. Winter *et al.*⁶ estimated the minimum thickness of the aqueous layer separating the tamponade fluid from the retina to be of the order of 5–10 μm . Vitreous substitute–aqueous interface breakdown may occur both at the wall (in correspondence of this thin film)^{7,8} and at the tamponade fluid–aqueous free interface where, in the case of incomplete filling of the vitreous chamber, the thickness of the aqueous pocket can be quite large, see Fig. 1.

Several clinical studies have investigated the conditions leading to the formation of an emulsion. It is generally believed that shear stresses at the tamponade fluid–aqueous interface generated during eye rotations play a crucial role on the generation of the interface instability.^{7,9} This problem remains, however, poorly understood from the mechanical point of view and no modeling approaches have yet been attempted to investigate it.

We speculate that, if the interface breakdown is originated at the wall, it can indeed be related to shear flow instability at the interface between the tamponade fluid and the aqueous. If, on the other hand, it occurs at the free interface between the two fluids, in the case of incomplete filling of the vitreous chamber, other physical mechanisms might play a role, such as sloshing. We focus in this paper on the possible role of shear flow instability.

Obviously, the generation of an emulsion is a highly nonlinear process that cannot be understood through a linear stability analysis. However, it seems conceptually relevant to investigate the role that each of the physical quantities involved in the problem has in producing the instability of the vitreous replacement fluid–aqueous interface, which we regard as a possible very initial step toward emulsification.

Owing to the lack of understanding of this instability process, we consider a highly idealized problem that, in our view, represents the suitable starting point to understand the basic mechanisms underlying the instability process. We consider a flat solid surface representing the vitreous chamber wall (located at $y^* = 0$), performing sinusoidal oscillations along the x^* direction, see Fig. 2. Throughout the paper, superscript asterisks denote dimensional variables. We assume that two immiscible fluids occupy the region of space $y^* \geq 0$. The interface between the two fluids is at $y^* = d^*$; fluid 1 (representing the aqueous) occupies the region $0 \leq y^* \leq d^*$, and fluid 2 (representing the vitreous substitute) extends in the y^* direction from d^* to infinity. This geometrical

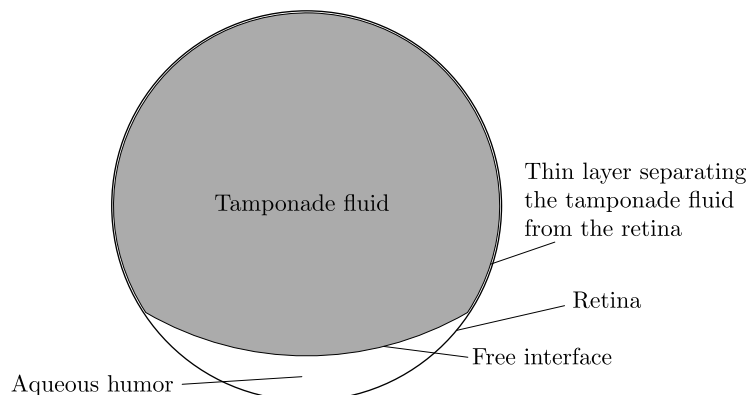


FIG. 1. Schematic sketch of a cross-section on the vitreous chamber filled with a tamponade fluid.

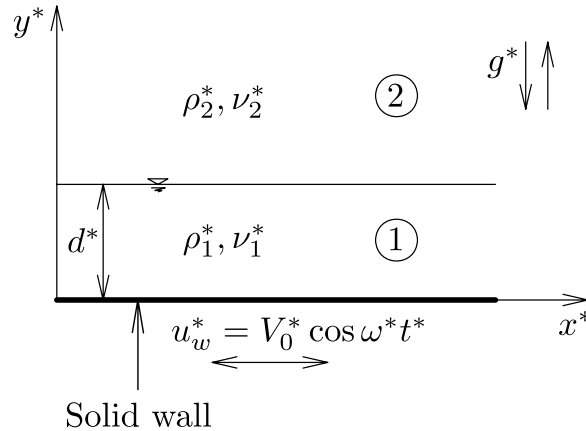


FIG. 2. Sketch of the geometry considered and notation. Note that gravity can act both in the positive and negative directions of y^* , depending on the orientation of the wall.

configuration represents well the real case when the thickness of the aqueous layer is much smaller than the radius of the eye, so that the curvature is negligible and the retina can be thought of as a flat surface. Obviously, real eye movements are not exactly harmonic in time. However, a sequence of saccadic rotations in opposite directions can be roughly thought of as a periodic harmonic movement. This is what has been assumed in most theoretical and experimental studies of vitreous humor dynamics (see for instance Refs. 10–15). Moreover, assuming harmonic oscillations of the plate allows us to find an analytical solution of the basic flow.

The idealized problem shown in Fig. 2 resembles studies which can be found in the literature. Most of these studies^{16–21} are based on the so-called quasi-steady approach and/or a Floquet analysis. In the quasi-steady approach, the linear stability problem is solved by “freezing” the basic flow at each instant in time and the method is valid when the frequency of the basic flow is much smaller than that of the perturbation. This cannot be known *a priori* and must be verified from the numerical results. The Floquet analysis, on the other hand, does not depend on the aforementioned scale separation. In the quasi-steady approach, it is possible to find unstable solutions during an interval within the oscillating cycle of the basic flow. However, this does not necessarily imply that amplification of the perturbation is sustained over the whole period.

In the limit in which density and viscosity of the two fluids are the same and the surface tension vanishes, we obtain the case of the flat Stokes layer. Results^{16–18} show that the critical Reynolds number, based on the displacement thickness of the boundary layer, is less than 200 in the case of the quasi-steady approach while the Floquet analysis gives a critical Reynolds number of about 708.

Several investigations^{19–21} concern one or more fluids above an oscillating wall. The most pertinent cases, in relation to the current study, are the investigations by Yih¹⁹ and Or,²⁰ who studied the stability of a single fluid layer over an oscillating flat wall. In the case of quasi-steady flow conditions and long waves Yih was the first to find that instability occurs during certain phases of the cycle if $\omega^2 Re^2/5 > Fr^{-2}$, where Re is the Reynolds number and Fr is the Froude number, both according to the definitions given in Sec. II.

The paper is organized as follows: In Sec. II, we formulate the mathematical problem and estimate the range of variation of the dimensionless parameters involved. We then show the results of the stability analysis in Sec. III. Finally, discussion and conclusions follow in Sec. IV.

II. FORMULATION OF THE MATHEMATICAL PROBLEM

We consider two immiscible and incompressible fluids occupying the regions of space $0 \leq y^* < d^*$ and $y^* > d^*$, respectively, with densities ρ_1^* and ρ_2^* and dynamic viscosities μ_1^* and μ_2^* . The flow is induced by periodic motion of the rigid wall located at $y^* = 0$ (see Fig. 2), and the oscillation

is described by

$$u_w^* = V_0^* \cos(\omega^* t^*) = \frac{V_0^*}{2} (e^{i\omega^* t^*} + c.c.), \quad (1)$$

where V_0^* is a velocity representing the amplitude of the oscillations, t^* is time, ω^* is the angular frequency, and $c.c.$ denotes the complex conjugate. Let \mathbf{u}_i^* be the velocity vector and p_i^* the pressure, where the index i is taken to be equal to 1 for the fluid closer to the wall and 2 for the other fluid.

The governing equations are made dimensionless using V_0^* , d^* , ρ_1^* as reference velocity, length, and density, respectively. The dimensionless variables can therefore be written

$$\mathbf{x} = \frac{\mathbf{x}^*}{d^*}, \quad \mathbf{u}_i = \frac{\mathbf{u}_i^*}{V_0^*}, \quad p_i = \frac{p_i^*}{\rho_1^* V_0^{*2}}, \quad t = \frac{V_0^*}{d^*} t^*, \quad \omega = \frac{d^*}{V_0^*} \omega^*, \quad (2)$$

where $\mathbf{x} = (x, y, z)$ is the vector of spatial coordinates with x, y , and z being the streamwise, wall-normal, and spanwise coordinates, respectively. The stability analysis is performed by introducing a decomposition of the solution of the governing equations as

$$\mathbf{u}_i = \mathbf{U}_i + \bar{\mathbf{u}}_i, \quad p_i = P_i + \bar{p}_i, \quad (3)$$

where capital letters indicate the basic flow and small letters with a bar refer to perturbation quantities.

A. Basic flow

We consider the case in which the basic flow is laminar and fully developed in the streamwise direction. The solution, $\mathbf{U}_i = [U_i(y, t), 0, 0]$ ($i = 1, \dots, 2$) is obtained by solving the following system of non-dimensional equations:

$$\frac{\partial U_1}{\partial t} = \frac{1}{Re} \frac{\partial^2 U_1}{\partial y^2}, \quad (4a)$$

$$\frac{\partial P_1}{\partial y} = -Fr^{-2}, \quad (4b)$$

$$\frac{\partial U_2}{\partial t} = \frac{m}{\gamma} \frac{1}{Re} \frac{\partial^2 U_2}{\partial y^2}, \quad (4c)$$

$$\frac{\partial P_2}{\partial y} = -\gamma Fr^{-2}, \quad (4d)$$

where $Re = V_0^* d^* \rho_1^* / \mu_1^*$ is the Reynolds number, $Fr = \frac{V_0^*}{\sqrt{g^* d^*}}$ is the Froude number, $m = \mu_2^* / \mu_1^*$ is the ratio between the dynamic viscosities, and $\gamma = \rho_2^* / \rho_1^*$ between the densities. The boundary conditions impose that the fluid velocity at the wall is given by Eq. (1), that continuity of velocity and stress is satisfied at the interface and that the velocity vanishes at infinity. The pressure has hydrostatic distribution and the solution for the velocities U_1 and U_2 is readily found to be

$$U_1 = [c_1 e^{-ay} + c_2 e^{ay}] e^{i\omega t} + c.c., \quad (5a)$$

$$U_2 = c_3 e^{-by} e^{i\omega t} + c.c., \quad (5b)$$

where

$$a = \sqrt{i\omega Re}, \quad (6a)$$

$$b = \sqrt{\frac{\gamma}{m} i\omega Re}, \quad (6b)$$

$$c_1 = \frac{e^{a-b}}{2[e^{a-b}(a+mb) + e^{-a-b}(a-mb)]}, \quad (6c)$$

$$c_2 = \frac{e^{-a-b}}{2[e^{a-b}(a + mb) + e^{-a-b}(a - mb)]}, \tag{6d}$$

$$c_3 = \frac{a}{e^{a-b}[mb + a] + e^{-a-b}[mb - a]}. \tag{6e}$$

At the beginning of Sec. II, we defined the characteristic scales adopted to make our governing equations dimensionless. In particular, we use the thickness of the layer d^* as the characteristic length, in analogy to what was done in previous similar works.¹⁹⁻²¹ In other investigations involving a single fluid and, specifically, in the literature on the stability of the Stokes boundary layer, it is common to use as reference length scale the thickness of the boundary layer at the wall, $\delta^* = \sqrt{2\nu_1^*/\omega^*}$. In order to allow one to easily compare our findings with those relative to the stability of the Stokes layer, we provide below expressions for converting one set of dimensionless parameters into the other. Denoting Re_S and α_S the Reynolds number and streamwise wavenumber for the Stokes boundary layer case, we obtain

$$Re_S = \frac{1}{2} \frac{\delta^*}{d^*} Re, \quad \alpha_S = \alpha \frac{\delta^*}{d^*}, \quad \text{where} \quad \frac{\delta^*}{d^*} = \sqrt{\frac{2}{\omega Re}}. \tag{7}$$

B. Linear stability analysis

The governing equations for the linear stability analysis are derived adopting a quasi-steady approach, i.e., it is assumed that perturbations evolve on a time scale that is significantly smaller than the characteristic scale of the basic flow. This implies that we study the stability of a “frozen” basic flow at time τ , with $0 \leq \tau < 2\pi/\omega$. The suitability of this approach can be verified *a posteriori* by checking the relative magnitude of the time scale of perturbations with respect to that of the basic flow.

It is well known from Squire’s theorem that, for a steady parallel shear flow, the flow first becomes unstable to two-dimensional perturbations.²² The validity of this theorem has also been shown for quasi-steady flows.²³ Thus, we consider only two-dimensional perturbations, so that $\bar{\mathbf{u}}_i = (\bar{u}_i, \bar{v}_i, 0)$. This allows us to introduce the stream functions

$$\bar{u}_i = \frac{\partial \bar{\psi}_i}{\partial y}, \quad \bar{v}_i = -\frac{\partial \bar{\psi}_i}{\partial x}. \tag{8}$$

Taking advantage of the infinite extension of the domain in streamwise direction, we expand the solution in Fourier modes as

$$\bar{\psi}_i = e^{i\alpha(x-\Omega t)}\psi_i(y, \tau) + c.c., \tag{9}$$

where α is the real-valued dimensionless wavenumber and Ω is the complex-valued phase velocity. Stable and unstable solutions are defined by $\Im(\Omega) < 0$ and $\Im(\Omega) > 0$, respectively.

Moreover, let $\bar{\eta}$ denote the dimensionless perturbation of the interface position, measured in units of d^* . We impose

$$\bar{\eta} = \eta(\tau)e^{i\alpha(x-\Omega t)} + c.c. \tag{10}$$

The governing stability equations are derived by introducing the flow decomposition (3), stream functions (8), and solution forms (9) and (10) into the Navier–Stokes equations, and neglecting nonlinear perturbation terms. The two equations, one for each fluid, read

$$\psi_1'''' - 2\alpha^2\psi_1'' + \alpha^4\psi_1 + i\alpha Re \left[\psi_1 \frac{\partial^2 U_1}{\partial y^2} - U_1(\psi_1'' - \alpha^2\psi_1) \right] = -i\alpha Re\Omega(\psi_1'' - \alpha^2\psi_1), \tag{11a}$$

$$\psi_2'''' - 2\alpha^2\psi_2'' + \alpha^4\psi_2 + \frac{i\alpha\gamma}{m} Re \left[\psi_2 \frac{\partial^2 U_2}{\partial y^2} - U_2(\psi_2'' - \alpha^2\psi_2) \right] = -\frac{i\alpha\gamma}{m} Re\Omega(\psi_2'' - \alpha^2\psi_2), \tag{11b}$$

where the superscript ‘ denotes derivation with respect to y and the basic flow velocity U_i is computed at the generic time τ . The above equations have to be solved subject to the following

boundary conditions:

$$\psi_1 = 0 \quad (y = 0), \quad (12a)$$

$$\psi_1' = 0 \quad (y = 0), \quad (12b)$$

$$U_1\eta + \psi_1 = \Omega\eta \quad (y = 1), \quad (12c)$$

$$\psi_1' + \eta \frac{\partial U_1}{\partial y} = \psi_2' + \eta \frac{\partial U_2}{\partial y} \quad (y = 1), \quad (12d)$$

$$\psi_1'' + \alpha^2\psi_1 + \eta \frac{\partial^2 U_1}{\partial y^2} = m \left(\psi_2'' + \alpha^2\psi_2 + \eta \frac{\partial^2 U_2}{\partial y^2} \right) \quad (y = 1), \quad (12e)$$

$$i\alpha Re (\psi_1 U_1' - U_1 \psi_1') - i\alpha Re (\psi_2 U_2' - U_2 \psi_2') + (\psi_1''' - 3\alpha^2\psi_1') - m(\psi_2''' - 3\alpha^2\psi_2') - i\alpha^3 Re S\eta = -i\alpha Re \Omega (\psi_1' - \psi_2') \quad (y = 1), \quad (12f)$$

$$\psi_2 = 0 \quad (y \rightarrow \infty), \quad (12g)$$

$$\psi_2' = 0 \quad (y \rightarrow \infty), \quad (12h)$$

with $S = \frac{\sigma^*}{\rho_1^* d^* V_0^{*2}}$ being the dimensionless surface tension, where σ^* represents the dimensional surface tension.

Conditions (12a) and (12b) are the no-slip conditions at the wall. Continuity of the tangential and normal components of the velocity at the interface is enforced by (12c) and (12d). Condition (12e) imposes the continuity of the tangential stress at the interface and (12f) states that the difference between the normal stresses across the interface is balanced by surface tension. Finally, (12g) and (12h) enforce vanishing velocity as $y \rightarrow \infty$. Note that, owing to linearization, the conditions at the interface are imposed in the undisturbed position of the surface, $y = 1$.

The above system of Eqs. (11) and (12) has been discretized using a second-order finite-difference scheme on discrete points with constant spacing. Boundary conditions (12g) and (12h) are enforced using standard asymptotic inviscid solutions. The discrete system can be written as a generalized eigenvalue problem

$$A\mathbf{v} = \Omega B\mathbf{v}, \quad (13)$$

where $\mathbf{v} = (\psi_1, \eta, \psi_2)^T$. The solution of (13) is found using an inverse iterative approach.

The physical solution of the linear stability problem is given as a function of the discrete Fourier modes obtained from the solution of Eq. (13). It is well known^{17,24,25} that the solution of the linear stability problem of parallel flows in semi-infinite domains is composed of a set of discrete modes and a continuous spectrum. This is true also in this case. The eigenfunctions corresponding to the discrete modes have their maximum value within the boundary layer, while the continuous modes are traveling waves which are bounded far from the wall and decay in time.

A grid convergence study was performed and the domain size and resolution were chosen such that the eigenvalue had an error of less than 1%. Further, the solution of the numerical code was compared with results found in Yih,¹⁹ who studied the stability of a single fluid layer over an oscillating flat wall. In the case of quasi-steady flow conditions and long waves, he found that instability occurs during certain phases of the cycle if $\omega^2 Re^2/5 > Fr^{-2}$. We checked our numerical solution in the limit $\gamma \rightarrow 0$ and $\alpha \rightarrow 0$ against this analytic result, finding excellent agreement.

C. Energy analysis

In this section, we explore the evolution of the disturbance kinetic energy of the two-fluid system. An equation for the kinetic energy is obtained by first taking the scalar product between the velocity vector and the linearized Navier-Stokes equations, and then integrating over the respective domain \mathcal{V}_i . For a given volume, the energy is defined as $E_i = \frac{1}{2} \int_{\mathcal{V}_i} \frac{\bar{\mathbf{u}}_i \cdot \bar{\mathbf{u}}_i}{2} d\mathcal{V}_i$ and the total disturbance kinetic energy is given by

$$E = E_1 + \gamma E_2. \quad (14)$$

In vector form, the evolution equation for the disturbance kinetic energy, for the domain \mathcal{V}_i , reads

$$\frac{dE_i}{dt} = - \int_{\mathcal{V}_i} \bar{\mathbf{u}}_i \cdot (\nabla \mathbf{U}_i) \bar{\mathbf{u}}_i d\mathcal{V}_i - \frac{1}{Re} \int_{\mathcal{V}_i} \bar{\mathbf{u}}_i \cdot \Delta \bar{\mathbf{u}}_i d\mathcal{V}_i + \int_S \bar{\mathbf{u}}_i \cdot \bar{\boldsymbol{\sigma}}_i \bar{\mathbf{n}} dS, \tag{15}$$

where $\bar{\boldsymbol{\sigma}}_i$ is the stress tensor, S denotes the surface of the interface, and Δ denotes the Laplacian operator. The first term on the right hand side of the above expression is the contribution due to the base flow shear, the second is due to dissipation, and the third to the interface between the two fluids. Some conclusions regarding these three integrals can be drawn if (15) is rewritten using integration by parts and Gauss' theorem. The resulting equation, in primitive variable form reads

$$\begin{aligned} \frac{\alpha}{2\pi} \frac{dE}{dt} = & - \int_0^1 u_1 v_1 U_1' dy - \gamma \int_1^{+\infty} u_2 v_2 U_2' dy \\ & - \frac{1}{Re} \int_0^1 \left[\left(\frac{\partial u_1}{\partial x} \right)^2 + \left(\frac{\partial u_1}{\partial y} \right)^2 + \left(\frac{\partial v_1}{\partial x} \right)^2 + \left(\frac{\partial v_1}{\partial y} \right)^2 \right] dy \\ & - \frac{m}{Re} \int_1^{+\infty} \left[\left(\frac{\partial u_2}{\partial x} \right)^2 + \left(\frac{\partial u_2}{\partial y} \right)^2 + \left(\frac{\partial v_2}{\partial x} \right)^2 + \left(\frac{\partial v_2}{\partial y} \right)^2 \right] dy \\ & \left(v_1 [(\gamma - 1) Fr^{-2} + \alpha^2 S] \eta - \frac{v_1}{Re} \left(\frac{\partial v_1}{\partial y} - m \frac{\partial v_2}{\partial y} \right) + \frac{1}{Re} \left(u_1 \frac{\partial u_1}{\partial y} - m u_2 \frac{\partial u_2}{\partial y} \right) \right) \Big|_{y=1}. \end{aligned} \tag{16}$$

Inspection of Eq. (16) shows that the dissipation terms are always negative, thus they invariably have a damping effect on the energy evolution. We further note that the effect of the interface disappears in the case when $S = 0$, $\gamma = 1$, and $m = 1$, i.e., the case of a single fluid.

By definition, the growth rate $\Im(\Omega)$ obtained from the solution of Eq. (13) is equal to the logarithmic derivative of the disturbance kinetic energy

$$\frac{1}{2\alpha E} \frac{dE}{dt} = \text{Im}(\Omega). \tag{17}$$

Therefore, by multiplying the left and right-hand side of Eq. (16) with $\pi/(\alpha^2 E)$ we can compare the contributions to the total growth rate from the individual terms in the right hand side of (16).

D. Estimation of the range of variability of the dimensionless parameters

In this section, we estimate the range of variation of the dimensionless parameters Re , ω , m , γ , Fr , and S , that govern the stability problem, referring to the ocular application that motivates this work. Saccadic eye rotations are the fast movements performed when the direction of sight is redirected from one target to another. Becker²⁶ reports that the relationship between saccade duration T^* and saccade amplitude A is well described by the following linear relationship:

$$T^* = T_0^* + t^* A, \tag{18}$$

with $t^* \approx 0.0025$ s/deg and $0.02 \leq T_0^* \leq 0.03$ s. In (18), the amplitude A has to be expressed in degree. In this work, we approximate a sequence of eye rotations by describing the eye wall velocity as a sinusoidal function of time, according to (1). Assuming that this periodic motion is the result of successive eye rotations in opposite directions we can estimate a relationship between the frequency and the amplitude of eye rotations as $\omega^* = 2\pi/(2T^*)$, with T^* computed from Eq. (18). Since, owing to (1), $A = V_0^*/(\omega^* R_{\text{eye}}^*)$, with $R_{\text{eye}}^* \approx 0.01$ m being the radius of the eye, this establishes a relationship between the dimensionless parameters Re and ω , which is plotted in Fig. 3(a). The different curves in the figure correspond to different values of the thickness of the aqueous layer d^* ; each point of the curves refers to a different value of the amplitude A , with small values of ω corresponding to large amplitude rotations.

The density and viscosity of the aqueous humor are approximately equal to those of water, thus we assume $\rho_1^* = 10^3$ kg/m³ and $\nu_1^* = 10^{-6}$ m²/s.

Vitreous substitutes are characterized by physical properties varying in a very wide range. In this paper, we do not focus on the behavior of a particular vitreous substitute. Rather, we investigate the role of the mechanical properties of the fluid on the instability mechanism. Thus, we will vary

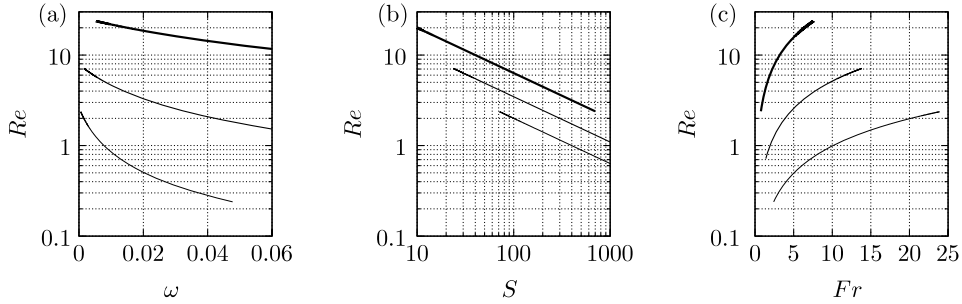


FIG. 3. Relationship between Re and ω (a), S (b) and Fr (c) obtained adopting feasible values for eye movements. From thin to thick curves: $d^* = 1 \times 10^{-5}$ m, $d^* = 3 \times 10^{-5}$ m, $d^* = 1 \times 10^{-4}$ m. Each point on the curves corresponds to a different value of A .

the parameters m and γ within a fairly large range of values ($1 \leq m \leq 200$, $0.8 \leq \gamma \leq 2$). We note, however, that in the case of silicon oils much higher values of the ratio m than those considered here can be attained.

We finally note that, once values for d^* and σ^* are prescribed, relationships between Re and S , Fig. 3(b), and between Re and Fr , Fig. 3(c), can be established.

III. RESULTS

We first consider pure shear instability and neglect the effect of density differences between the two fluids, thus assuming $\gamma = 1$. Note that in the equations governing the stability problem, the Froude number only appears in the boundary condition (12f), where it is multiplied by $(1 - \gamma)$. Therefore Fr does not play a role in the stability of the system when the two fluids have the same density.

In order to determine baseline values for the dimensionless parameters, we assume that the layer of fluid 1 has a thickness $d^* = 3 \times 10^{-5}$ m, and that the dimensional surface tension is $\sigma^* \approx 0.02$ N/m. The actual value of the surface tension between silicon oils used in vitreoretinal surgery and aqueous humor can vary within a relatively wide range, owing to the possible presence of surfactants. Here we have chosen a relatively small value for σ^* that is representative of what happens in patients who develop oil emulsification, in which cases surfactants are likely to be present.²⁷ Referring to the curves reported in Fig. 3, we assume as baseline values $Re = 7$, $\omega = 0.001$, and $S = 14$. We note that in all cases discussed in the following $\alpha \Re(\Omega)$ (which is a measure of the dimensionless frequency of perturbations) is significantly larger than ω , thus ensuring the separation of time scales required for the quasi-steadiness approach to be valid (see Figure 8 and the related discussion). Employing Eq. (7) from the above dimensionless parameters, we can compute the values of the Reynolds number Re_S and of the streamwise wavenumber α_S , based on the use of the thickness of the boundary layer as the characteristic length, which is the usual choice in the analysis of the Stokes layer. We find $Re_S = 59$, $L_S = 2\pi/\alpha_S \approx 0.06L$.

In Fig. 4, we show neutral stability curves, i.e., curves on which $\Im(\Omega) = 0$, on the plane $(\omega t/\pi) - L$, where $L = 2\pi/\alpha$ is the dimensionless wave length of the perturbation. Each curve corresponds to a different value of the ratio between fluid viscosities m , and all other dimensionless parameters are kept fixed. In the range of values of the parameters shown in the figures, sufficiently long waves are linearly unstable during certain phases of the basic flow cycle. Note, however, that in all cases shown in the figure, the interface is stable during most time instants. Whether amplification will actually occur, over one or more periods, depends on the value of the growth rate and on the initial magnitude of perturbations.

By definition, the growth rate computed with the energy analysis presented in Sec. II C coincides with that computed solving the eigenvalue problem (13). However, the energy analysis allows us to obtain a better insight on the mechanisms governing the instability. In Fig. 5, we show how the various contributions to the energy change appearing in Eq. (16) depend on L , for a given time

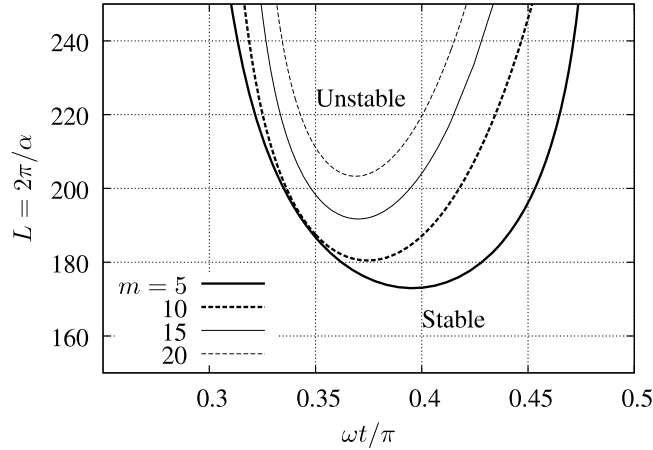


FIG. 4. Neutral stability curves in the $(\omega t/\pi) - L$ plane for different values of the parameter m ($= 5, 10, 15, 20$). $Re = 7$, $\omega = 0.001$, $S = 14$, $\gamma = 1$.

(Fig. 5(a)) and on ωt , for a given perturbation wave length (Fig. 5(b)). In the figure, we also plot the growth rate $\Im(\Omega)$, suitably scaled to fit in the plot ($\Im(\Omega)$ has been multiplied by 300). The figure shows that the leading energy production term is related to the existence of the interface, i.e., the term computed in $y = 1$ in Eq. (16). Note that this contribution vanishes when $m = 1$, $S = 0$, and $\gamma = 1$, i.e., when a single fluid is present.

In Fig. 6, we show the effect of changing the ratio m between the two fluid viscosities. In the figure, we plot the value of the growth rate $\Im(\Omega)$ versus m , for different values of the perturbation length L . As the value of m increases, the minimum length of unstable waves grows. However, there exists a value of m (≈ 21.6) for which a maximum value of $\Im(\Omega)$ is attained. Thus increasing m has a twofold effect: on one hand short waves are stabilized, on the other hand, for relatively small values of m ($\lesssim 21.6$), the system becomes effectively more unstable, since the growth rate also increases. For $m \gtrsim 21.6$, further increase of the ratio between the fluid viscosities has an overall stabilizing effect.

In Figs. 7(a) and 7(b), we investigate the effect of modifying the values of S and R (keeping m fixed and equal to 5). In particular, we show how the shortest unstable wavelength changes with these parameters. As one would intuitively expect, when the surface tension parameter S is decreased, the flow becomes more unstable, in the sense that progressively shorter waves become unstable. In a similar manner, the flow becomes more unstable if the Reynolds number is increased.

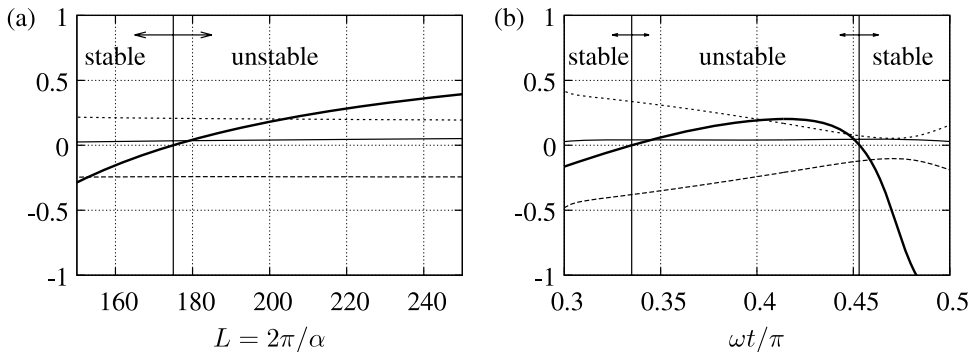


FIG. 5. Contributions to the perturbation energy growth versus L for $\omega t/\pi = 0.4$ (a) and $\omega t/\pi$ for $L = 200$ (b) (see Eq. (16)). Thin solid curve: volume integral production term. Dashed curve: volume integral dissipation term. Dotted curve: surface integral on the interface. In the figures, we also report with a thick solid curve the growth rate as computed solving the eigenvalue problem (13), suitably scaled for readability. This curve allows one to distinguish stable and unstable regions in the plot. In both figures $Re = 7$, $S = 14$, $m = 5$.

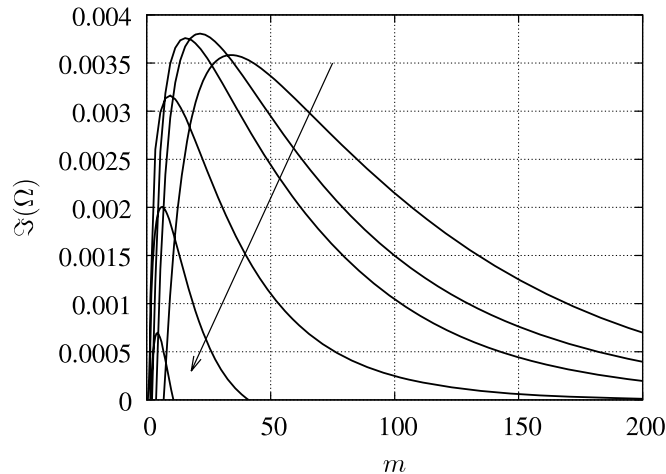


FIG. 6. Growth rate $\mathfrak{I}(\Omega)$ versus m for different values of the perturbation length L ($= 200, 300, 500, 800, 1000, 1400$). The arrow points to decreasing values of L . $\omega = 0.001$, $Re = 7$, $S = 14$, $\gamma = 1$.

We finally consider the effect of changing the value of γ . Obviously, if the lighter fluid is on top, the effect of gravity is to stabilize the interface. We therefore focus on cases in which the aqueous layer is very thin and the heavier fluid is on top. This means that we consider either the lower portion of the vitreous chamber when a heavier than water vitreous substitute is adopted, or the upper region of the retina when a lighter than water fluid is used. As discussed in the Introduction, these situations are believed to possibly occur in practice.^{7,8,27} Fig. 7(c) shows that if γ increases, the system moves toward instability, again meaning with this statement that progressively shorter waves are found to be unstable.

IV. DISCUSSION AND CONCLUSIONS

In this paper, we have considered the geometry depicted in Fig. 2 and studied the linear stability of the interface between the two immiscible fluids 1 and 2, assuming that fluid motion is induced by periodic oscillations of the solid wall along the x^* -direction. We have adopted a quasi-steady approach, thus assuming that perturbations evolve on a time scale which is shorter than the time scale of evolution of the basic flow.

We first considered the case in which the two fluids have the same density and different viscosities ($\gamma = 1$, $m \neq 1$). The linear stability analysis shows that, for the range of the controlling parameters considered, long enough waves are linearly unstable during certain phases of the cycle.

A value of the ratio $m = \mu_2^*/\mu_1^*$ between the viscosities of the two fluids exists for which the instability of the interface is maximized. When m is large enough or when the viscosities of the two

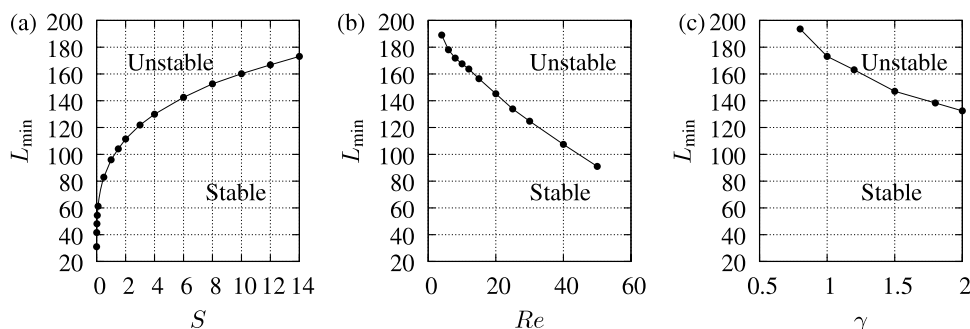


FIG. 7. Length of the shortest unstable perturbation L_{\min} versus S (a), Re (b), and γ (c) with $\omega = 0.001$ and $m = 5$. The values of $Re = 7$ in (a) and (c), $S = 14$ in (b) and (c), and $\gamma = 1$ in (a) and (b), respectively.

fluids are almost matching, the system is found to be stable, in the range of values of the controlling parameters considered here.

Investigation of the dependency of results on the other controlling parameters has shown that the system can be destabilized either by decreasing the surface tension parameter S or increasing the Reynolds number characteristic of the flow. We have also considered the effect of changing the ratio γ between fluid densities. In particular, we have focused on the case in which the heavier fluid is on top. As expected, in this case the system moves toward instability. Among the considered dimensionless parameter, those with a larger influence on the stability of the system are found to be the ratio m between fluid densities and the surface tension parameter S .

The present work is motivated by the need of understanding the stability conditions of the interface between the aqueous humor layer close to the retina and a vitreous substitute in vitrectomized eyes. We have adopted a highly idealized geometry and fluid flow structure, which obviously, represent a gross simplification of the fluid dynamics inside of a real eye. However, our idealized geometry can provide insight on the onset of the aqueous–vitreous substitute interface instability in the case in which the thickness of the aqueous layer is much smaller than the eye radius and perturbations are not too long. We note that no theoretical models have been proposed so far to explain, on mechanical grounds, the onset of the aqueous–vitreous substitute interface instability. Therefore, this exploratory work, in spite of the significant simplifying assumptions it is based on, represents a suitable starting point to understand the mechanics of this problem. In particular, we believe, it has the strength of allowing us to assess the role of all parameters involved in the instability mechanism.

We now discuss whether and to what extent the present results can be directly applied to interpret and predict the occurrence of the vitreous substitute–aqueous humor breakdown in eyes.

We first note that our findings are in qualitative agreement with empirical observations, to which they therefore provide a sound physical foundation. In particular, our results are in agreement with the observation that highly viscous vitreous substitutes are more resistant to emulsification than less viscous ones.^{28–30} Moreover, the stabilizing role of the surface tension parameter is in agreement with empirical observations,^{31,32} according to which the tendency to emulsification is significantly enhanced by the presence of surfactants that decrease the surface tension between the two fluids. Finally, the model predicts that the system becomes more unstable as the Reynolds number of the flow is increased, which explains why patients with increased eye mobility are more prone to develop emulsification.³³ Notwithstanding the fact that the stabilizing role of surface tension and the destabilizing role of the Reynolds number are not surprising from the mechanical point of view, the model allows us to quantify their effect.

Throughout the paper as baseline dimensional values we have assumed $d^* = 3 \times 10^{-5}$ m for the thickness of the aqueous layer and $\sigma^* = 0.02$ N/m for the surface tension between the two fluids. Based on these values, Fig. 7(a) shows that the shortest unstable perturbation has a dimensional wavelength $L^* = Ld^* \approx 5$ mm. This value has to be compared with the radius of the eye ($R_{\text{eye}}^* \approx 12$ mm). Following the above estimates, our model's direct applicability to the eye might be questioned, since the length of the shortest unstable wave is not much smaller than the eye radius and, therefore, additional effects that have been neglected here, such as the sphericity of the domain, might not be negligible. Results, however, show that once additional effects are accounted for (possibly in combination to one another), such as, in particular, changes in the surface tension, increased eye mobility, or gravitational effects in the case in which the heavier fluid is on top of the lighter one, the wavelength of unstable perturbations is small enough for the model to be a good representation of the real case. Thus we can conclude that shear instability is likely to be a possible mechanism triggering the onset of vitreous substitutes–aqueous interface instability.

Several other assumptions underlie the present work, which are listed and briefly discussed in the following.

- (i) Our stability analysis is based on the quasi-steady approach. In other words, we have assumed that a separation of time scales exists, such that perturbations evolve on a shorter time scale than the basic flow. This assumption holds in certain parameter regimes, on which we have focused our attention. In particular, this implies considering large amplitude and

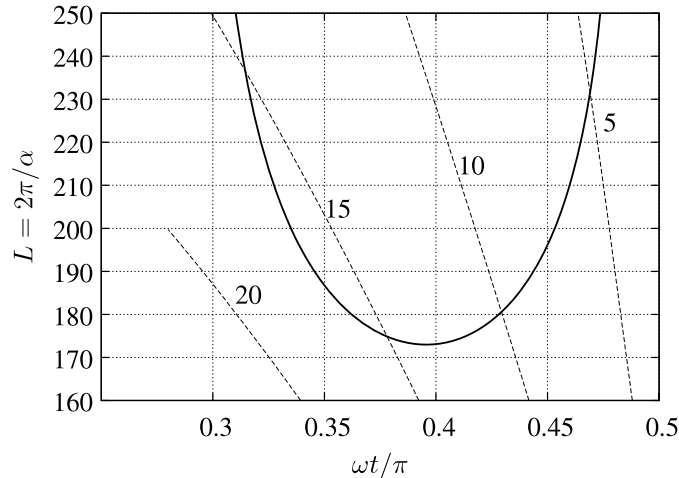


FIG. 8. Neutral stability curve (solid line) in the $(\omega t/\pi) - L$ plane for the case $m = 5$, $Re = 7$, $\omega = 0.001$, $S = 14$, $\gamma = 1$. The dotted lines show the values of the ratio $\alpha \mathfrak{R}(\Omega)/\omega$.

relatively low frequency eye rotations. In Fig. 8, we report a verification of the scale separation, by plotting the contour lines of the ratio $\alpha \mathfrak{R}(\Omega)/\omega$ of the perturbation frequency to the frequency of the basic flow (dashed curves). In the figure we also plot, with the solid line, the neutral stability curve corresponding to $m = 5$, the same as was shown in Fig. 4. As discussed earlier, in order for the assumption of scale separation to hold the ratio $\alpha \mathfrak{R}(\Omega)/\omega$ should be significantly larger than one in most of the unstable region. This is indeed shown to be the case in the figure. The same analysis has been carried out for all results shown in this paper (not shown here).

In order to account for high frequency oscillations of the wall, a stability analysis based Floquet's theory should be adopted,³⁴ an endeavor that we plan to undertake in the near future.

- (ii) We have assumed that the retina has a perfectly smooth surface. In reality, the retinal surface is characterized by a roughness that might have an amplitude comparable to the thickness of the aqueous layer, when the latter is very thin. The presence of this roughness is likely to contribute to the destabilization of the interface between the two fluids.
- (iii) We have assumed periodic rotations of the eye. Real eye rotations are not necessarily periodic and not sinusoidal in time. Adoption of a more realistic time law for the wall motion might have some influence on the results presented in this paper.
- (iv) We have focused our attention on the instability mechanism induced by shear between the two fluids. In the case of incomplete filling of the vitreous chamber with the vitreous substitute, a thick pocket of aqueous forms in the chamber (see Fig. 1). In this case, the interface instability can also be triggered by other physical mechanisms, such as sloshing.

Accounting for all complexities inherent to the real fluid motion inside an eye in the presence of vitreous replacement fluids would need a fully numerical approach to the problem. However, we strongly believe that stability analyses such as the one proposed here can contribute to highlight basic physical mechanisms and are an indispensable tool to guide and interpret more realistic numerical simulations.

¹ F. Kuhn and B. Aylward, "Rhegmatogenous retinal detachment: A reappraisal of its pathophysiology and treatment," *Ophthalmic Res.* **51**, 15 (2013).

² N. Soman and R. Banerjee, "Artificial vitreous replacements," *Bio-Med. Mater. Eng.* **13**, 59 (2003).

³ H. Heimann, T. Stappeler, and D. Wong, "Heavy tamponade I: A review of indications, use, and complications," *Eye (London, England)* **22**, 1342 (2008).

⁴ T. T. Kleinberg, R. T. Tzekov, L. Stein, N. Ravi, and S. Kaushal, "Vitreous substitutes: A comprehensive review," *Surv. Ophthalmol.* **56**, 300 (2011).

- ⁵ P. Ichhpujani, A. Jindal, and L. J. Katz, "Silicone oil induced glaucoma: A review," *Graefe's Arch. Clin. Exp. Ophthalmol.* **247**, 1585 (2009).
- ⁶ M. Winter, W. Eberhardt, C. Scholz, and A. Reichenbach, "Failure of potassium siphoning by müller cells: A new hypothesis of perfluorocarbon liquid-induced retinopathy," *Invest. Ophthalmol. Visual Sci.* **41**, 256 (2000).
- ⁷ D. J. de Silva, K. S. Lim, and W. E. Schulenburg, "An experimental study on the effect of encircling band procedure on silicone oil emulsification," *Br. J. Ophthalmol.* **89**, 1348 (2005).
- ⁸ Y. K. Chan, C. O. Ng, P. C. Knox, M. J. Garvey, R. L. Williams, and D. Wong, "Emulsification of silicone oil and eye movements," *Invest. Ophthalmol. Visual Sci.* **52**, 9721 (2011).
- ⁹ Y. Toklu, H. B. Cakmak, S. B. Ergun, M. A. Yorgun, and S. Simsek, "Time course of silicone oil emulsification," *Retina (Philadelphia, PA)* **32**, 2039 (2012).
- ¹⁰ T. David, S. Smye, T. Dabbs, and T. James, "A model for the fluid motion of vitreous humour of the human eye during saccadic movement," *Phys. Med. Biol.* **43**, 1385 (1998).
- ¹¹ R. Repetto, "An analytical model of the dynamics of the liquefied vitreous induced by saccadic eye movements," *Meccanica* **41**, 101 (2006).
- ¹² A. Stocchino, R. Repetto, and C. Cafferata, "Eye rotation induced dynamics of a newtonian fluid within the vitreous cavity: The effect of the chamber shape," *Phys. Med. Biol.* **52**, 2021 (2007).
- ¹³ J. Meskauskas, R. Repetto, and J. H. Siggers, "Oscillatory motion of a viscoelastic fluid within a spherical cavity," *J. Fluid Mech.* **685**, 1 (2011).
- ¹⁴ R. K. Balachandran and V. H. Barocas, "Contribution of saccadic motion to intravitreal drug transport: Theoretical analysis," *Pharm. Res.* **28**, 1049 (2011), ISSN 0724-8741.
- ¹⁵ M. Piccirelli, O. Bergamin, K. Landau, P. Boesiger, and R. Luechinger, "Vitreous deformation during eye movement," *NMR Biomed.* **25**, 59 (2012), ISSN 1099-1492, PMID: 21567512.
- ¹⁶ P. J. Blennerhassett and A. P. Bassom, "The linear stability of flat Stokes layers," *J. Fluid Mech.* **464**, 393 (2002).
- ¹⁷ P. Hall, "The linear-stability of flat Stokes layers," *Proc. R. Soc. London, Ser. A* **359**, 151 (1978).
- ¹⁸ C. V. Kerczek and S. H. Davis, "Linear stability theory of oscillatory Stokes layers," *J. Fluid Mech.* **62**, 753 (1974).
- ¹⁹ C.-S. Yih, "Instability of unsteady flows or configurations Part 1. Instability of a horizontal liquid layer on an oscillating plane," *J. Fluid Mech.* **31**, 737 (1968).
- ²⁰ A. C. Or, "Finite-wavelength instability in a horizontal liquid layer on an oscillating plane," *J. Fluid Mech.* **335**, 213 (1997).
- ²¹ C.-H. Li, "Instability of time-periodic flows of stratified fluids," *Phys. Fluids* **13**, 1121 (1970).
- ²² H. B. Squire, "On the stability for three-dimensional disturbances of viscous fluid flow between parallel walls," *Proc. R. Soc. London, Ser. A* **142**, 621 (1933).
- ²³ P. W. Conrad and W. O. Criminale, "The stability of time-dependent laminar flow: Parallel flows," *Z. Angew. Math. Phys.* **16**, 233 (1965).
- ²⁴ P. J. Schmid and D. S. Henningson, *Stability and Transition in Shear Flows* (Springer, Berlin, 2001).
- ²⁵ P. Hall, "On the instability of Stokes layers at high Reynolds numbers," *J. Fluid Mech.* **482**, 1 (2003).
- ²⁶ W. Becker, *The Neurobiology of Saccadic Eye Movements*, edited by R. H. Wurtz and M. E. Goldberg (Elsevier Science Publisher BV (Biomedical Division), 1989).
- ²⁷ M. E. Hammer, "Vitreous Substitutes," in *Duane's Ophthalmology 2013* (Lippincott Williams & Wilkins, 2012), ISBN 9781451187441.
- ²⁸ A. Crisp, J. de Juan, and E. J. Tiedeman, "Effect of silicone oil viscosity on emulsification," *Arch. Ophthalmol.* **105**, 546 (1987).
- ²⁹ H. Heidenkummer, A. Kampik, and S. Thierfelder, "Emulsification of silicone oils with specific physicochemical characteristics," *Graefe's Arch. Clin. Exp. Ophthalmol.* **229**, 88 (1991).
- ³⁰ H. P. Heidenkummer, A. Kampik, and S. Thierfelder, "Experimental evaluation of in vitro stability of purified polydimethylsiloxanes (silicone oil) in viscosity ranges from 1000 to 5000 centistokes," *Retina (Philadelphia, PA)* **12**, S28 (1992).
- ³¹ N. Savion, A. Alhalel, G. Treister, and E. Bartov, "Role of blood components in ocular silicone oil emulsification. Studies on an in vitro model," *Invest. Ophthalmol. Visual Sci.* **37**, 2694 (1996).
- ³² J. H. Dresch and D.-H. Menz, "Interaction of different ocular endotamponades as a risk factor for silicone oil emulsification," *Retina (Philadelphia, PA)* **25**, 902 (2005).
- ³³ T. Yilmaz and M. Güler, "The role of nystagmus in silicone oil emulsification after pars plana vitrectomy and silicone oil injection for complex retinal detachment," *Eur. J. Ophthalmol.* **18**, 150 (2008).
- ³⁴ P. Blennerhassett and A. P. Bassom, "On the linear stability of Stokes layers," *Philos. Trans. R. Soc., A* **366**, 2685 (2008).